CHAPTER 3

EXPERIMENTAL PROCEDURES

In this chapter, the experimental procedures employed for preparation and characterization of sol-gel derived thin films PZT, PZT/xWO$_3$ and PZT/xCuO (when x = 0, 0.1, 0.2, 0.3, 0.4, 0.5 and 1.0 wt%) Principles and measurement techniques of thermogravimetric analysis (TGA), differential thermal analysis (DTA), X-ray diffraction (XRD), scanning electron microscopy (SEM) and electrical properties such as dielectric, ferroelectric properties and fatigue are introduced, investigated and analyzed in the following sections.

3.1 Sample preparation

Fabrications of materials, including precursor preparation of PZT, PZT/WO$_3$ and PZT/CuO, and thin film fabrications of PZT, PZT/WO$_3$ and PZT/CuO were carried out as below.

3.1.1 Synthesis of sol-gel precursor

In this work, a PZT sol-gel precursor was prepared by a triol sol-gel route. All commercially available starting compounds used for the preparation of the compositions in this study are listed in Table 3.1, along with the suppliers, formula weights and purities.

Table 3.1 Chemicals used for the preparation of stock solution for preparation of (a) PZT and PZT/WO_3 and PZT/CuO by a triol sol-gel route and (b) PZT by a solid-state mixed oxide technique.

Powder	Chemical formula	Source	Formula weight	Purity (%)
(a) PZT by a triol sol-gel process				
- Zirconium (IV) propoxide	$Zr(OCH_2CH_2CH_3)_4$	Aldrich	327.58	70
- Acetylacetone	$C_5H_8O_2$	Fluka	100.12	99.5
- Titanium (IV) isopropoxide, TIAA	$C_{12}H_{28}O_4Ti$	Aldrich	284.27	97
- Lead (II) acetate trihydrate	$Pb(C_2H_3O_2)_2.3H_2O$	Riedel	379.33	99.99
- 1,1,1-tris (hydroxymethyl) ethane: THOME	$CH_3C(CH_2OH)_3$	Aldrich	120.15	99
- 2-Methoxyethanol	$CH_3OCH_2CH_2OH$	Aldrich	76.09	99.8
(b) PZT/WO_3 and PZT/CuO by a hybrid sol-gel process using PZT solution in part (a) and some metal oxide nano-particles which were:				
- Tungsten oxide (30-70 nm)	WO_3	Nanostructure & Amorphous Material	215.84	99+
- Copper Oxide (30-50 nm)	CuO		79.54	99+

A recirculation dry in N_2 glove box was used for storage and weighing of metal alkoxides and other moisture was necessary. The vessels were connected via rubber tubing to a dry N_2/vacuum line which enabled operations such as purging vessels and distillations at reduced pressure to be carried out under dry condition. Single layer PZT (of atomic ratio Zr/Ti = 52/48) thin films were prepared with 0, 5, 10 and 15 mol% of excess Pb by a triol sol-gel route [111] to find the optimum content of Pb excess. The starting materials used in this study were zirconium (IV) propoxide (70%, Aldrich) and acetylacetone (99%, Fluka) which were mixed in a dry nitrogen atmosphere as shown in Fig 3.1. The mixture was refluxed in an oil bath at 90 °C for 2 h (Fig 3.2). The solution was then cooled down to room temperature before adding titanium (IV) isopropoxide (99%, Aldrich), lead (II) acetate trihydrate (99.99%, Aldrich) and 1,1,1-tris (hydroxymethyl) ethane (99%, Aldrich) to the solution in order to reach the nominal stoichiometric composition of $Pb(Zr_{0.52}Ti_{0.48})O_3$. The mixture was then heated at 70 °C for 4 h. Before spin coating, the solution was diluted from 1.2 M to 0.75 M with 2-methoxyelthanol. The final product was a viscous golden solution, *so called* a sol. The sol preparation steps are shown in Fig. 3.3.

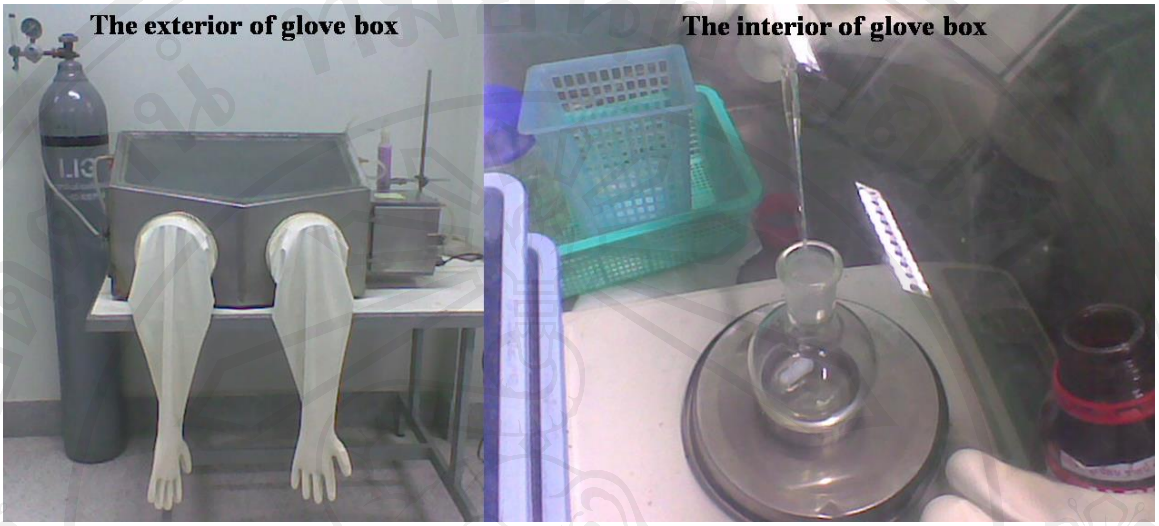

Figure 3.1 The glove box with dry nitrogen atmosphere for sol-gel preparation.

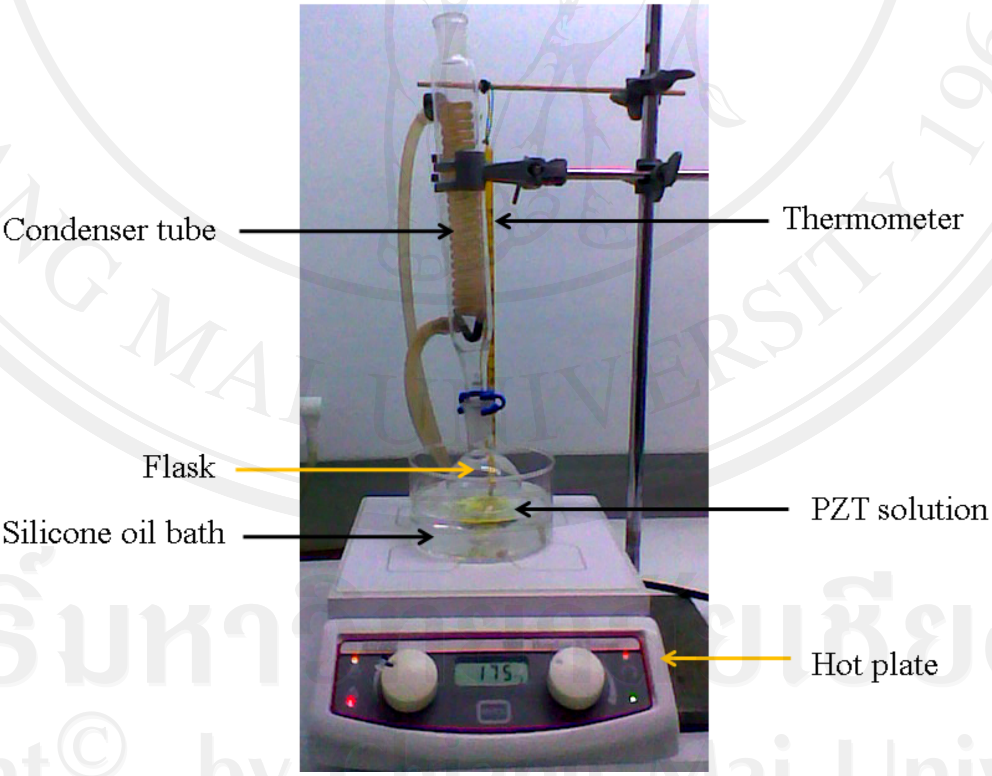

Figure 3.2 The mixture is refluxed in an oil bath.

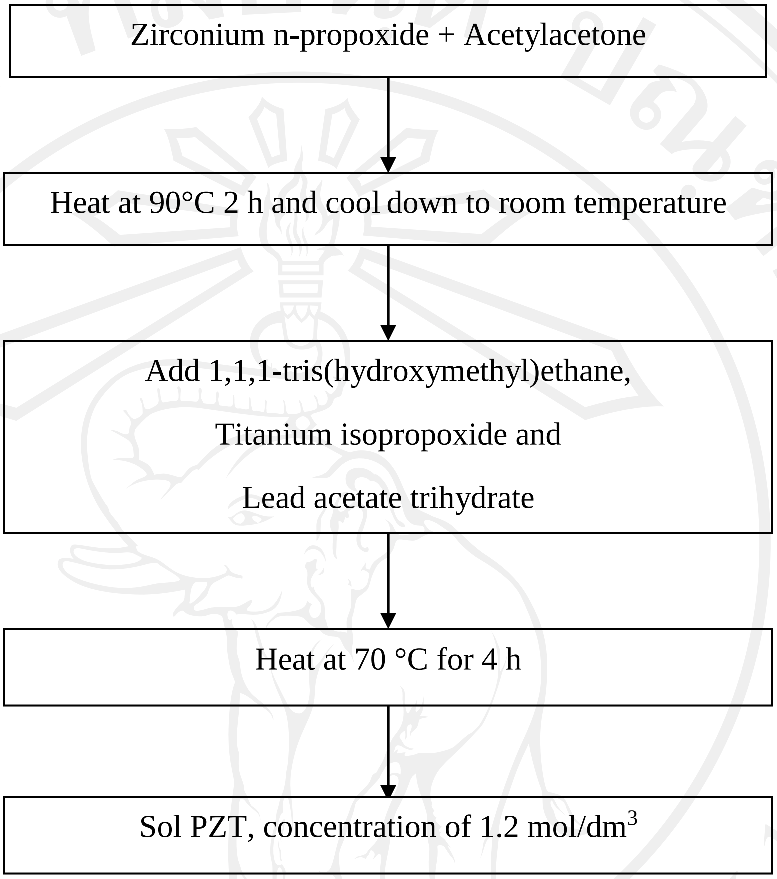

Figure 3.3 Flow diagram for preparation of PZT by triol sol-gel process

For preparation of PZT/WO_3 and PZT/CuO hybrid suspended solution, percentages by weight (0, 01, 0.2, 0.3, 0.4, 0.5 and 1) of WO_3 and CuO nanoparticles were ultrasonically dispersed in 2-methoxyethanol for 30 min before mixing with PZT precursor solution to stabilize solution and make a composite suspended solution as shown in Fig. 3.4.

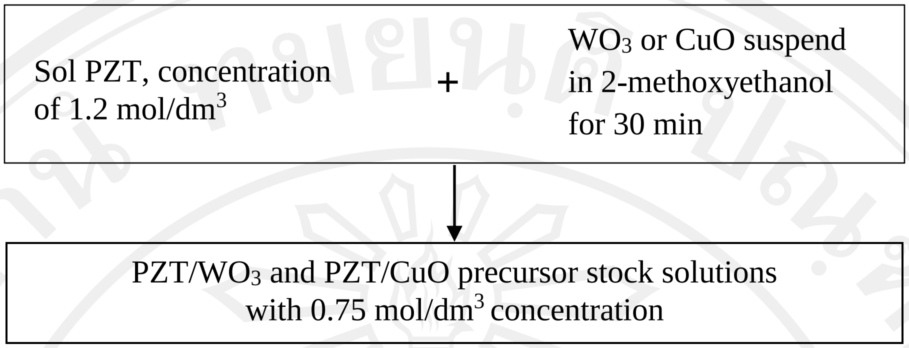

Figure 3.4 Flow diagram for preparation of PZT/WO$_3$ and PZT/CuO precursor stock solutions.

3.1.2 Fabrication of PZT thin film

PZT thin films were deposited on (111) preferred orientation platinised silicon substrates. A full configuration of the substrate was Pt/Ti/SiO$_2$/Si. The substrates used for film deposition were cut into 1 cm^2 and ultrasonically cleaned with a series of cleaning solvents, i.e. analar grade trichloroethylene, analar grade acetone and finally 2-propanol. Substrate preparation and subsequent film spinning and drying procedures were carried out in a clean room to minimize the problem of dust particles causing defects in the films. To spin coat, the PZT sols were filtered though a 0.2 μm Nylon 66 membrane filter. The films were prepared at a spin speed of 3000 rpm for 0.5 min [112]. The coated substrates were then heat treated on a custom built hotplate as shown in Fig. 3.5 (with temperature control unit) using various conditions as listed in Table 3.2 to study a phase of PZT films. After that, the flow diagram of heating step of PZT thin film fabrication was shown in Fig. 3.6 for study the microstructure of PZT thin films. In addition, the samples added by different excess Pb content of 0, 5, 10 and 15 mol % were also heat-treated using condition 5 in Table 3.2 then, all of them were study the phase by using X-ray diffractometry.

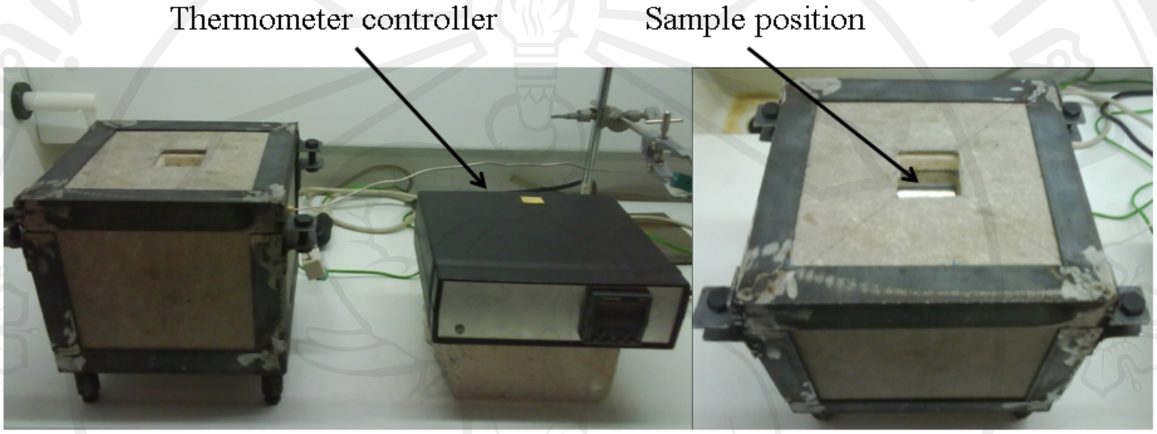

Figure 3.5 Custom built hotplate used in this work

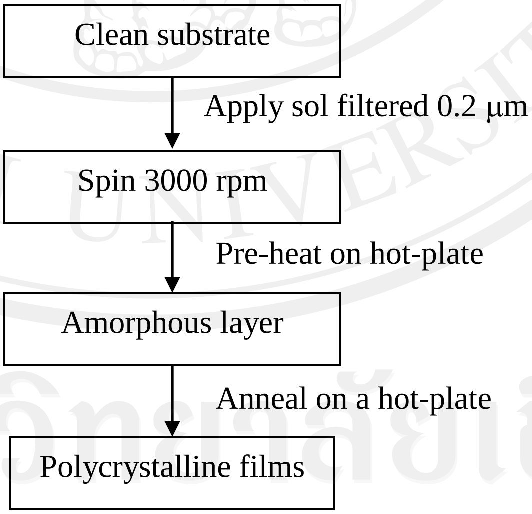

Figure 3.6 Flow diagram of thin film fabrication procedure

Table 3.2 Heat treated conditions for PZT thin films

Condition	Pre-heat temperature	Anneal temperature
1	200 °C/10 min	-
2	300 °C/10 min	-
3	400 °C/10 min	400 °C/30 min
4	400 °C/10 min	500 °C/30 min
5	400 °C/10 min	600 °C/30 min
6	400 °C/10 min	650 °C/30 min

To study the microstructure of PZT thin films, various heating steps (as shown in Fig. 3.7) were investigated by an optical microscope.

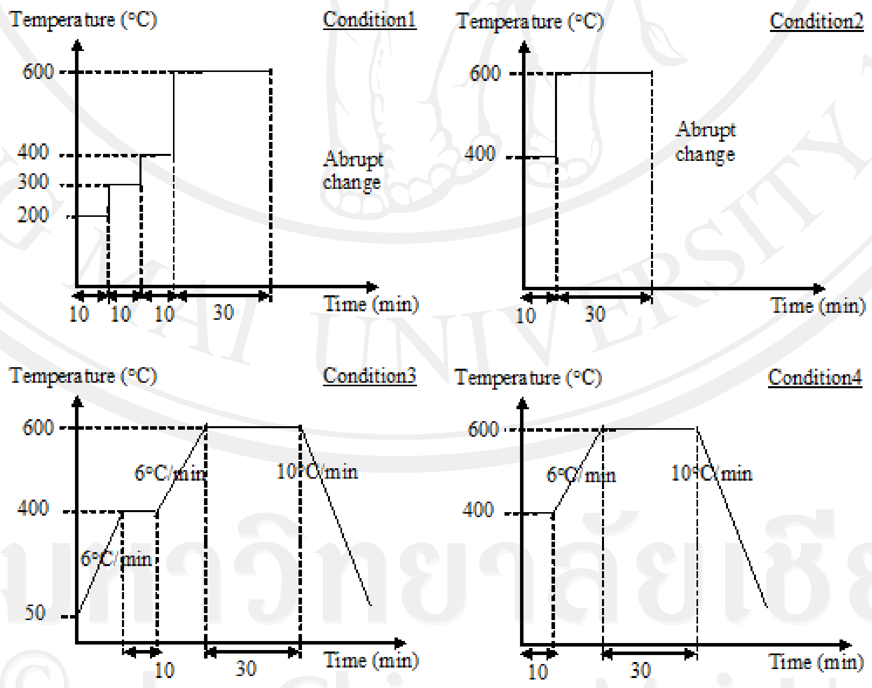

Figure 3.7 Various heating steps for microstructural study of PZT thin films.

3.1.3 Fabrication of PZT-based nanocomposite thin films

For preliminary investigation of processing condition of PZT-based nanocomposite precursors, WO_3 and CuO nanoparticles were weighted and ultrasonically dispersed into 2-methoxyethanol for 30 min, then poured into the sol PZT and stirred for 30 min. After that, PZT/WO_3 and PZT/CuO precursors were deposited on (111) preferred orientation platinised silicon substrates Pt/Ti/SiO_2/Si. As presented earlier, the substrates used for film deposition were cut into 1 cm^2 and ultrasonically cleaned with a series of cleaning solvents. The films were prepared at spin speed of 3000 rpm for 0.5 min. The coated substrates were then pre-heated at 400 °C for 10 min on a custom built hotplate. On the first layer of PZT/WO_3 or PZT/CuO, a subsequent layer of PZT solution (without WO_3 or CuO) was deposited. The pure PZT precursor solution can infiltrate into pores (or defects) in the composite film to increase the film density. Lastly, the composite film was heated again at 400 °C for 30 min with a final heat treatment carried out on a hot-plate at 600 °C for 30 min.

The optimum heat treatment conditions for prepare PZT-based nanocomposite thin films were explored using various conditions as listed in Table 3.3. The optimum heat treatment condition is a condition 7. This is described in the fabrication of PZT-based nanocomposite thin films process and the flow diagram of PZT/WO_3 nanocomposite thin film fabrication is shown in Fig. 3.8.

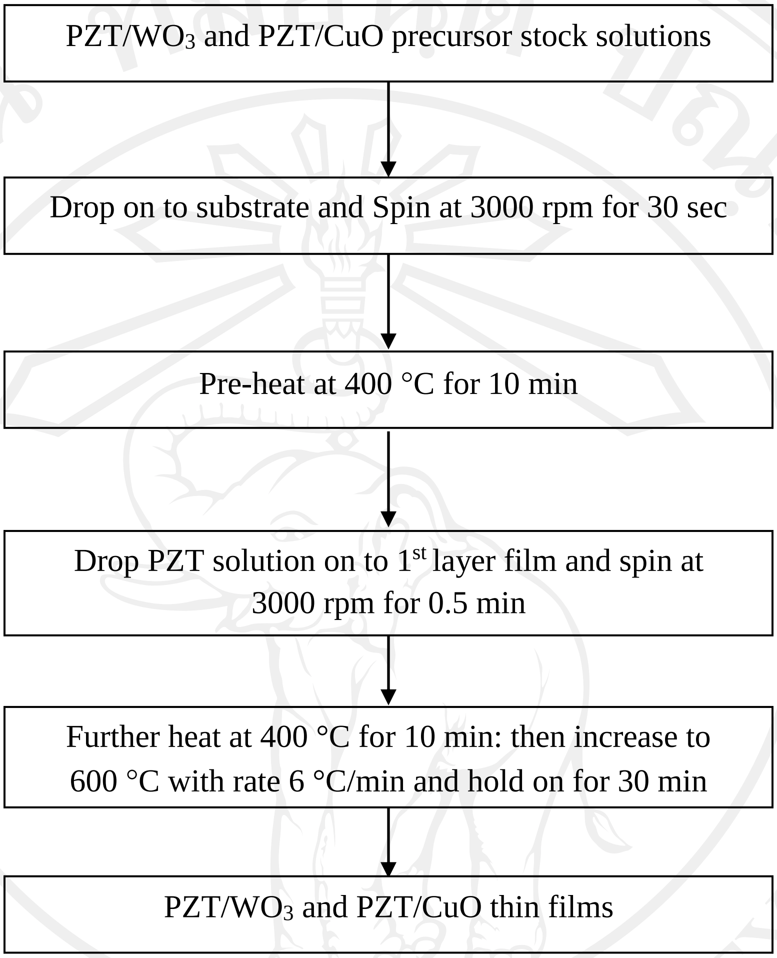

Figure 3.8 Flow diagrams for preparing PZT/WO_3 and PZT/CuO nanocomposite thin film.

Table 3.3 Heat-treat conditions for PZT-based nanocomposite thin films

Condition	Heating step for the 1st layer	Heating step for the 2nd layer
1	PZT/WO$_3$ 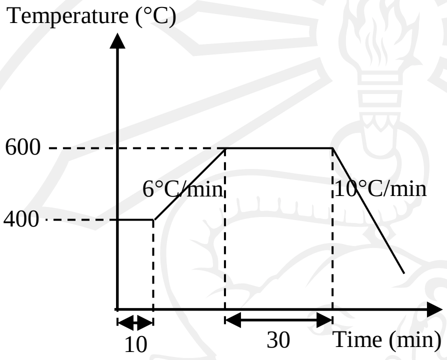	No layer
2	PZT/WO$_3$ 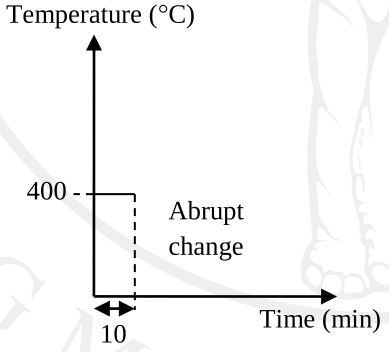	PZT/WO$_3$ 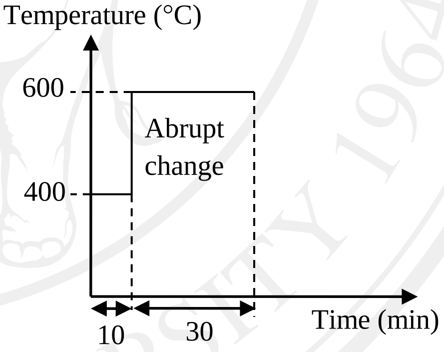
3	PZT/WO$_3$ 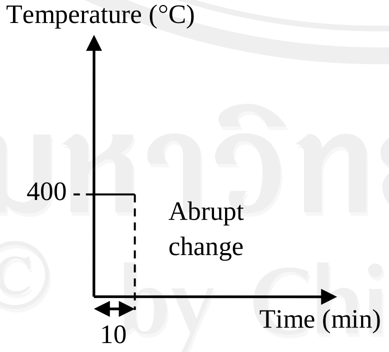	PZT/WO$_3$ 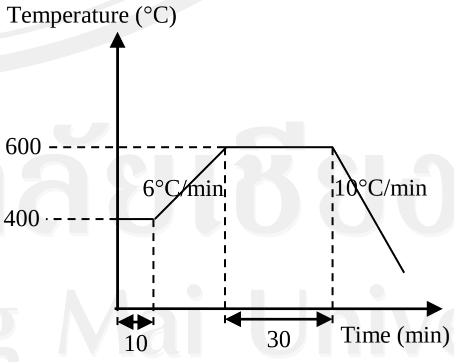

Table 3.3 Heat-treat conditions for PZT-based nanocomposite thin films (Continue)

Condition	Heating step for the 1st layer	Heating step for the 2nd layer
4	PZT/WO_3 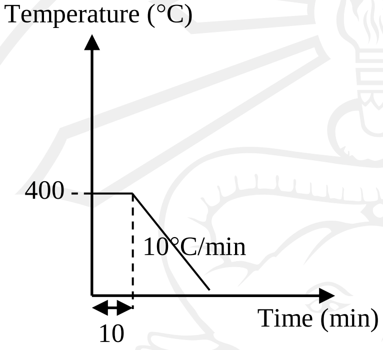	PZT/WO_3 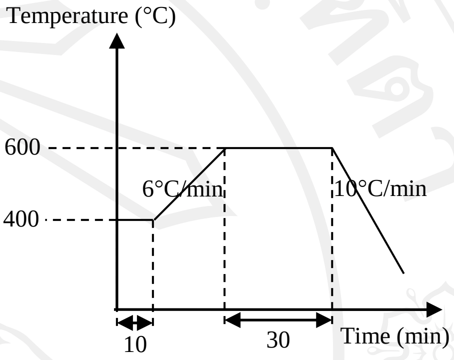
5	PZT/WO_3 No heat	PZT/WO_3 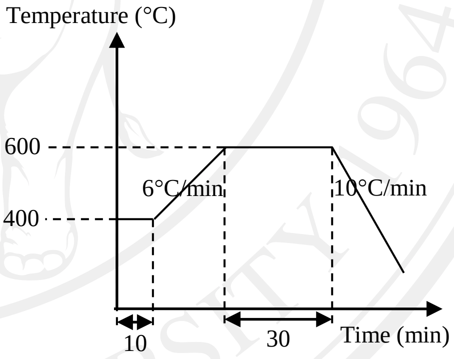
6	PZT/WO_3 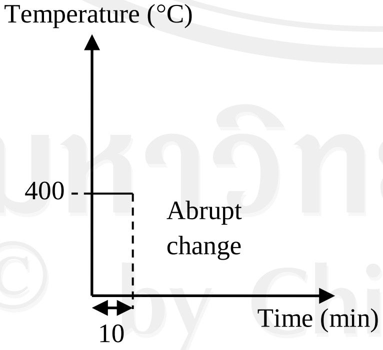	PZT 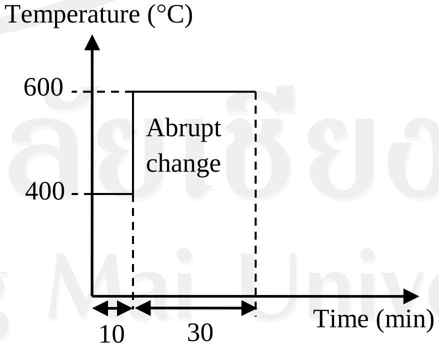

Table 3.3 Heat-treat conditions for PZT-based nanocomposite thin films (Continue)

Condition	Heating step for the 1st layer	Heating step for the 2nd layer
7	PZT/WO_3 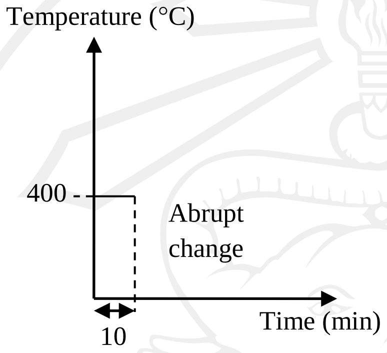 	PZT 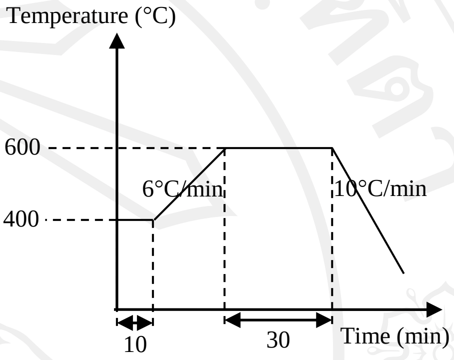
8	PZT/WO_3 No heat	PZT 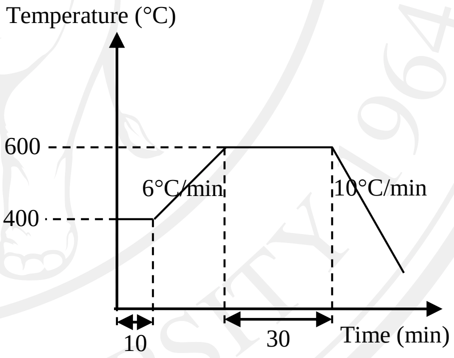

3.2 Sample characterization

Characterization techniques used for subsequent investigations of phase formation, microstructures, dielectric and ferroelectric properties are described in the following section.

3.2.1 Differential thermal analysis and thermogravimetric analysis

Differential thermal analysis (DTA) is a thermoanalytic technique similar to differential scanning calorimeter (DSC). In DTA, the study material and an inert reference need to have identical thermal cycles, while recording any temperature difference between sample and reference. This differential temperature is then plotted against time or against temperature (DTA curve or thermogram). Changes in the sample, either exothermic or endothermic, can be detected relative to the inert reference. Thus, a DTA curve provides data on the transformations that have occurred, such as glass transitions, crystallization, melting and sublimation. The area under a DTA peak is the enthalpy change and is not affected by the heat capacity of the sample [113].

Thermogravimetric Analysis (TGA) is a method of thermal analysis which measures the amount and rate of change in the weight of a material as a function of temperature or time in a controlled atmosphere. This technique uses heat to force reactions and physical change in materials. Measurements are used primarily to determine the composition of materials and to predict their thermal stability at temperatures up to about 1000 °C. The technique can characterize materials that exhibit weight loss or gain due to decomposition, oxidation, dehydration or transition. TGA also provides information about physical phenomena, such as second-order phase transitions, including vaporization, sublimation, absorption, adsorption, and desorption. Similarly, it provides chemical phenomena information including chemisorptions, desolvation (especially dehydration), decomposition and solid-gas reactions (e.g., oxidation or reduction) [114].

Thermal decomposition and weight loss behavior of as-synthesized PZT sol-gel which was dried in an oven at about 120 °C for 1 day and is grinded into powders before being analyzed by differential thermal analysis (DTA) and thermogravimetric analysis (TGA). These apparatuses are shown in Fig 3.9. In this experiment, EVISA Mettler Toledo AG-TGA/SDTA851e, EU was employed with platinum crucibles and Al_2O_3 as a reference powder with a heating rate of 10 °C/min. The decomposition temperature and weight loss were recorded when the powders were heated from room temperature to 800 °C.

Figure 3.9 TGA/SDTA851e horizontal type

3.2.2 X-ray diffraction

X-rays were discovered by Wilhelm Conrad Rontgen in 1895, just as the studies of crystal symmetry were being concluded. Physicists were initially uncertain of the nature of X-rays, although it was soon suspected that they were waves of electromagnetic radiation [115]. Finally, English physicists Sir W.H. Bragg and his son Sir W.L. Bragg argued that X-rays were not electromagnetic radiation, and they developed a relationship in 1913 to explain why the cleavage faces of crystals appear to reflect X-ray beam at certain angles of incidence (theta, θ) as shown in equation (2.1). The variable lambda λ is the wavelength of the incident X-ray beam; and n is an integer; the variable d is the distance between atomic layers in a crystal. All became Bragg's law as shown in equation below. This observation is an example of X-ray wave interference. Although Bragg's law was used to explain the interference pattern of X-rays scattered by crystals as shown in Fig. 3.10.

$$n\lambda = 2dsin\theta \tag{2.1}$$

X-ray crystallography is a method of determining the atomic and molecular structure of a crystal, in which the crystalline atoms cause a beam of X-rays to diffract into many specific directions. By measuring the angles and intensities of these diffracted beams, a crystallographer can produce a three-dimensional picture of the density of electrons within the crystal. From this electron density, the mean positions of the atoms in the crystal can be determined, as well as their chemical bonds, their disorder and various other information.

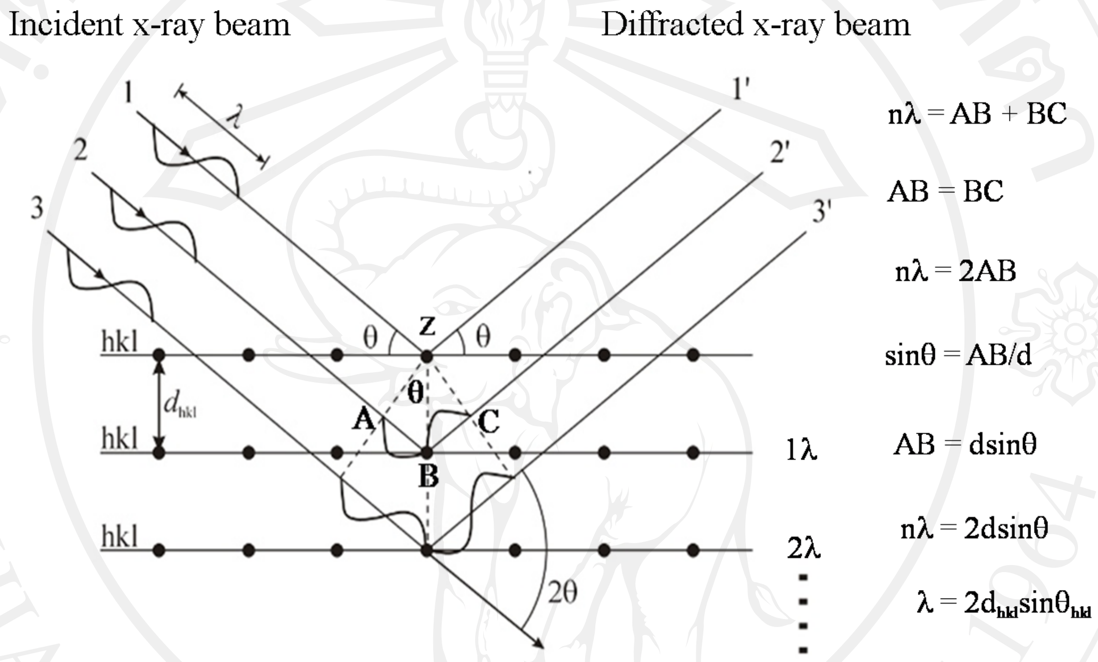

Figure 3.10 Bragg's Law reflection and derived [115]

Phases present in all films were finally characterized using X-ray diffractometry XRD; Bruger, D8 Discover, (Fig. 3.11) with a CuKα radiation X-ray source. Room temperature XRD data was recorded between 2θ range from 20° and 60° with a small angle technique (4° between X-ray beam and film) and step size of 2°/min. The XRD database of ICSD and JCPDS were used to determine the phase formation of the samples.

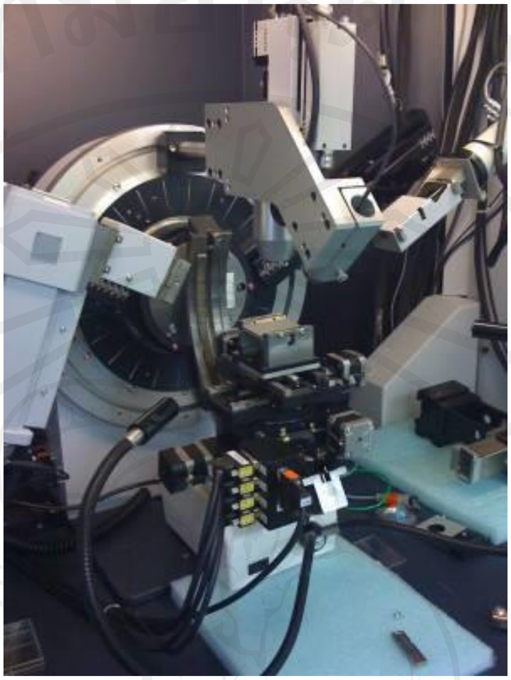

Figure 3.11 X-ray diffractometer (XRD; Bruger, D8 Discover)

3.2.3 Scanning electron microscopy

A scanning electron microscope (SEM) is a type of electron microscope that produces images of a sample by scanning it with a focused beam of electrons. The electrons interact with electrons in the sample, producing various signals that contain detectable information about the sample's surface topography and composition [116].

The types of signals produced by SEM include secondary electrons (SE), back-scattered electrons (BSE), characteristic X-rays, light (cathodoluminescence) (CL), specimen current and transmitted electrons. The signals result from interactions of the electron beam with atoms at or near the surface of the sample. In the most common or standard detection mode is secondary electron imaging or SEI, SEM can produce very high-resolution images of a sample surface, revealing details less than 1 nm in size. Due to the very narrow electron beam, SEM micrographs have a large depth of field, yielding a characteristic three-dimensional appearance useful for understanding the surface structure of a sample. A wide range of magnifications can be acquired, from about 10 times to more than 500,000 times (250 times is the magnification limit of the best light microscopes).

Back-scattered electrons (BSE) are beam electrons that are reflected from the sample by elastic scattering. BSE are often used in analytical SEM along with the spectra made from the characteristic X-rays, because the intensity of the BSE signal is strongly related to the atomic number (Z) of the specimen. BSE images can provide information about the distribution of different elements in the sample. Characteristic X-rays are emitted when the electron beam removes an inner shell electron from the sample, causing a higher-energy electron to fill the shell and release energy. These characteristic X-rays are used to identify the composition and measure the abundance of elements in the sample.

In this work, the scanning electron microscope (SEM, JEOL JSM-6335F, Fig. 3.12), was used to determine the morphology of the surface of films. The samples were cleaned by ultrasonic cleaner and coated with carbon sputtering (Fig. 3.13). During image acquisition, secondary electron modes were used with an accelerating voltage of 15 kV. The range of grain size and average grain size were determined by using the linear intercept method to the SEM micrographs.

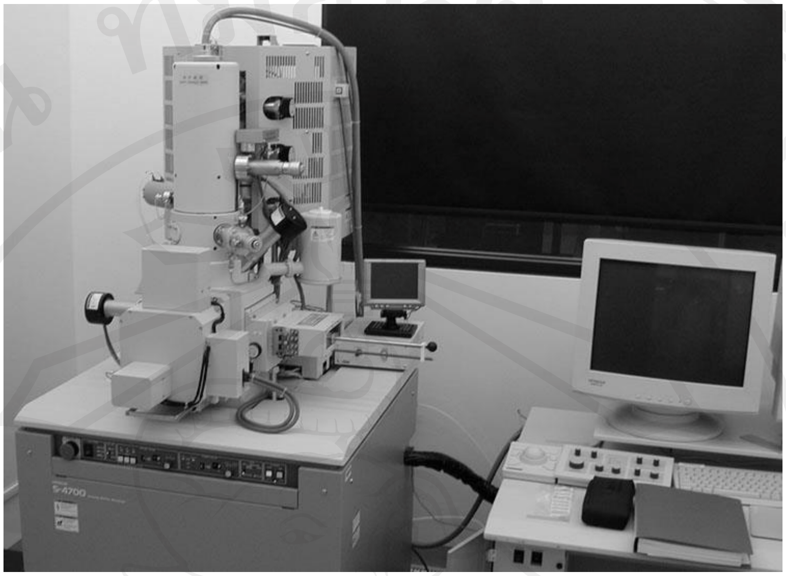

Figure 3.12 Scanning electron microscope

Figure 3.13 Sputter coater (JFC-1100E)

3.2.4 Dielectric measurement

For dielectric measurement, thicknesses of the films are required. The film's thicknesses were measured by an ellipsometer technique as shown in Fig 3.14. This equipment used an optical technique for thickness measurement by a change of reflective index upon the reflection or transmission. Before measurement, the films were coated with silver as electrodes by a thermal evaporator system as shown in Fig 3.15. Before placing the films in a sputtering chamber, the bottom electrode was made by etching one corner of the film with HF solution, and then put on an electrode mask (electrode size is about 7.85×10^{-9} m^2) on top of the films as shown in Fig 3.16. Finally, the samples were tested with a digital multimeter to check the quality of the electrodes. The dielectric properties were examined with an automated dielectric measurement system, LCZ-meter (Hewlett Packard 4192A, Fig. 3.17). The capacitance and the dielectric loss tangent were determined at room temperature with the frequency 1-1000 Hz. The dielectric constant (ε_r) was then calculated by the following equation:

$$\varepsilon_r = \frac{Cd}{\varepsilon_0 A} \tag{3.2}$$

where C is the capacitance of the sample (F),

ε_0 is the dielectric permittivity of vacuum (8.854×10^{-12} F/m),

A is the area of the electrode of the sample (m^2),

d is the thickness of the sample (m).

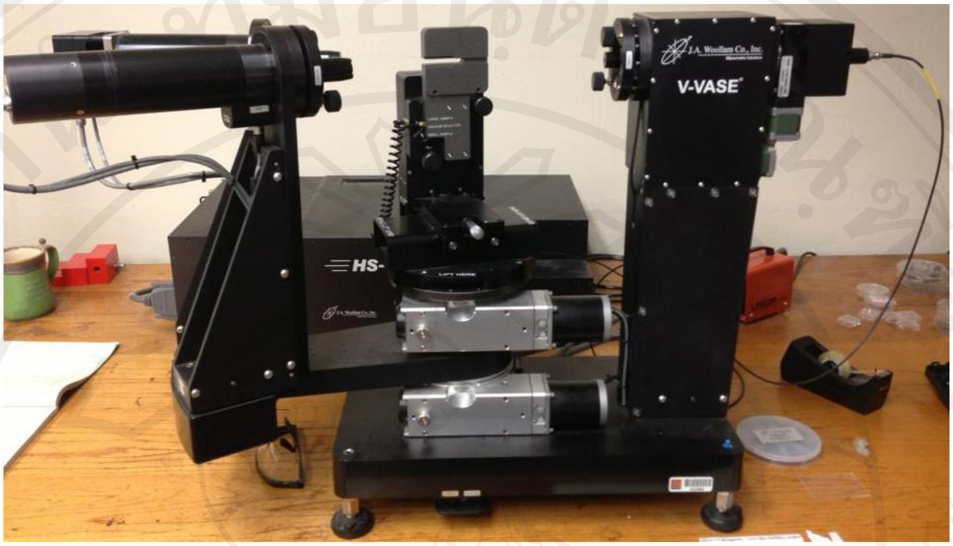

Figure 3.14 Ellipsometers (Ellipsometry solutions V-VASE, J.A. Woollam)

Figure 3.15 Thermal evaporator systems

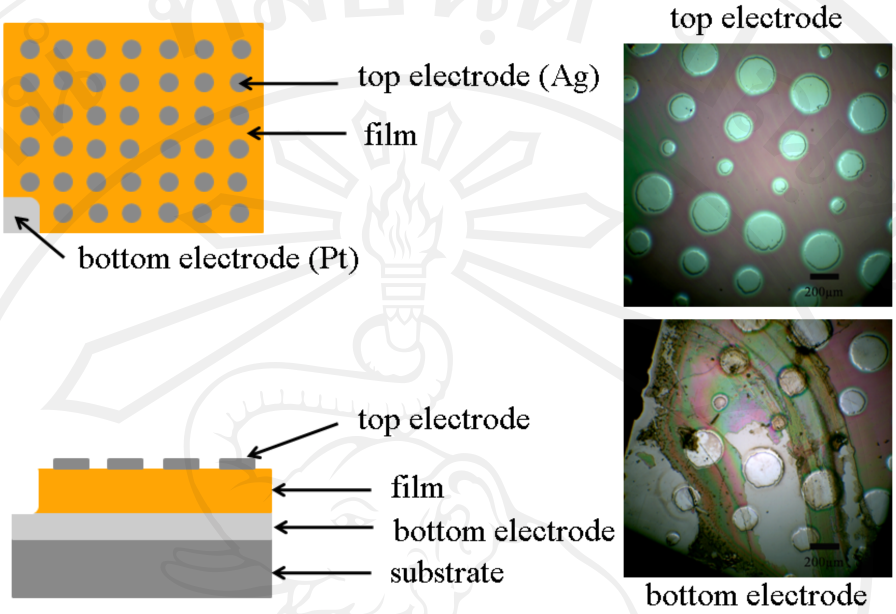

Figure 3.16 The film electrode made by a thermal evaporation technique.

Figure 3.17 LCZ meters for dielectric properties measurement at room temperature

3.2.5 Ferroelectric measurement

After making the films' electrode with silver using thermal evaporator technique as described earlier. The ferroelectric hysteresis (*P*-*E*) loops were characterized using a computer controlled and modified Sawyer-Tower circuit. The electric field was applied to a sample by a high voltage AC amplifier with the input sinusoidal signal at fixed measuring frequency of 50 Hz from a function generator. The *P*-*E* loops were recorded by a digital oscilloscope. The system is an automated device intended primarily to measuring the polarization of materials induced by an electric field with ferroelectric standard tester (The Precision RT66B Model, Radiant Technology, Fig. 3.18). For each measurement, the samples were placed on the probe station (Fig. 3.19) and then connected to the ferroelectric standard tester. Since the capacitance of the sample was much smaller than that of the standard capacitor, almost all the electric potentials of the high voltage source acted on the sample.

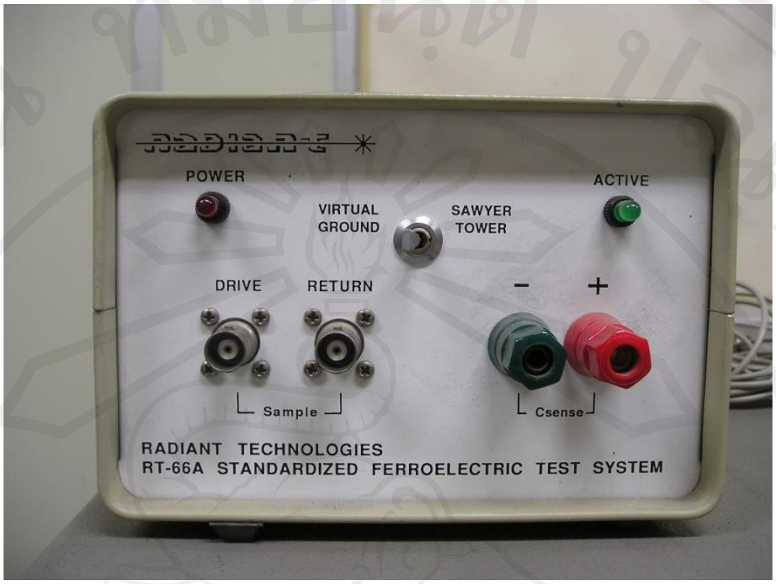

Figure 3.18 Radiant technology standardized ferroelectric test system

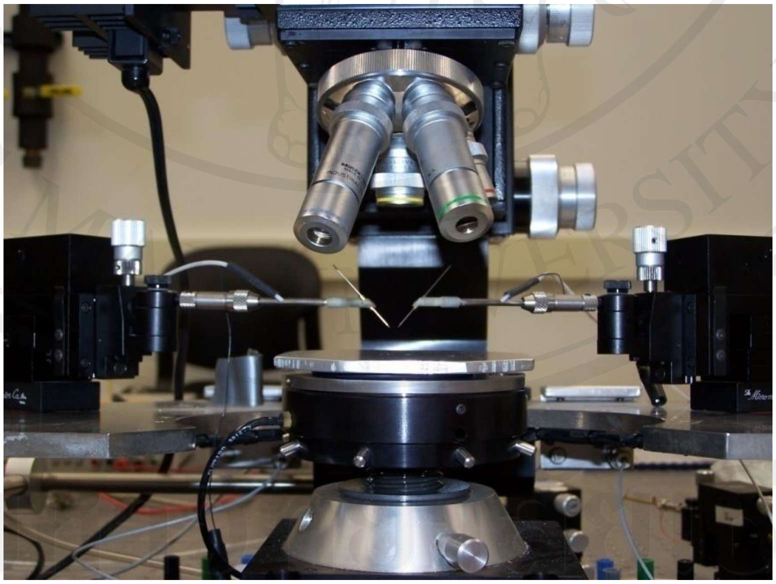

Figure 3.19 Probe station for electrical measurement of thin films

By definition, polarization is the value of dipole moment per unit volume or amount of charge accumulated per unit surface area. Polarization of the sample induced by electric field loading, P_{sample} was given by:

$$P_{sample} = \frac{Q_s}{A} \tag{3.3}$$

where Q_s is the amount of charges accumulated on the electrode of the sample (C)

A is the area of the electrode of the sample (cm^2).

Since the reference capacitor was connected in series to the sample, the amount of charges are equivalent:

$$Q_s = Q_0 \tag{3.4}$$

where Q_0 is the amount of charges accumulated on the standard capacitor (C).

On the other hand, the amount of charges on the standard capacitor is equal to:

$$Q_0 = V_y C_0 \tag{3.5}$$

where V_y is the voltage across the standard capacitor (V), and

C_0 is the capacitance of the standard capacitor (1 μF).

The polarization induced by electric field loading was then calculated using the following equation:

$$P_{sample} = \frac{V_y C_o}{A} \tag{3.6}$$

Consequently, by monitoring the voltage across the standard capacitor, the polarization of the sample can be determined.

From the *x*-axis of the monitor of oscilloscope, the electric field was calculated using the following equation:

$$E = \frac{V_x}{d} \tag{3.7}$$

where E is the electric field applied to the sample (V/cm),

V_x is the voltage across the circuit (V), and

d is the thickness of the sample (cm).

3.2.6 Fatigue measurement

Ferroelectric ceramics have been widely employed in many applications, such as electromechanical sensors, transducers and actuators. One critical problem that limits the device performance is the fatigue degradation associated with the electric cycling [117]. The reduction in amplitude of the polarization hysteresis due to electric fatigue is a well known phenomenon in bulk as well as thin film [118]. Fatigue rate is defined a change in remanent polarization as a function of the number of switching cycles. The remanent polarization (P_r), the polarization which appears when the applied electric field is zero, was selected to examine the characteristics of fatigue behavior. For fatigue measurement, the loading conditions were obtained from the sample as the fatigue rate is affected by the loading conditions.

After having determined the films thickness by using ellipsometer, the film's electrode was made with silver using thermal evaporator technique. Then, the ferroelectric hysteresis (*P-E*) loops were measured using a Sawyer-Tower circuit as described above. From the saturation loops, 3 times of a switching electric field (E_{sw}) were selected to study electrical fatigue. Thus, in this research, the loading conditions of fatigue measurement were fixed. The films were fatigued under applied electric field of 3 times of a switching electric field of saturation loop (E_{max}). The fatigue behavior was recorded up to 10^8 cycles. The polarization fatigue tests were performed using a triangular pulsed electric field of 500kV/cm at 1 kHz. All the changes were given as percentages of remanent polarization.